Applied Materials Today 22 (2021) 100894

Contents lists available at ScienceDirect

Applied Materials Today

journal homepage: www.elsevier.com/locate/apmt

Observation of giant persistent photoconductivity on vanadium dioxide thin film device

Gi Yong Lee[a], Bongjin Simon Mun[b,c,*], Honglyoul Ju[a,*]

[a] Department of Physics, Yonsei University, Seoul 120-749, Republic of Korea
[b] Department of Physics and Photo Science, Gwangju Institute of Science and Technology, Gwangju 61005, Republic of Korea
[c] Center for Advanced X-ray Science, Gwangju Institute of Science and Technology, Gwangju 61005, Republic of Korea

ARTICLE INFO

Article history:
Received 6 October 2020
Revised 11 November 2020
Accepted 24 November 2020

Keywords:
Giant persistent photoconductivity
Vanadium dioxide
Insulator-to-metal transition
Laser induced ultrafast switching devices

ABSTRACT

We report a giant persistent photoconductivity (GPPC) phenomenon in VO_2 film device prepared on corning glass substrate. With a single pulse laser irradiation onto the device at bias voltages of 7 V and 8 V, the VO_2 film makes an insulator-to-metal transition with a sharp increase of photo current. The photo current remained at a highly conductive state for long period, e.g. the photo current for VO_2 device was decreased only ~1% in one day. The GPPC was found within the limit of critical voltages of the hysteresis loop in voltage vs current curve of the device. High speed time-current measurements on the device with a 20 ms single pulse laser irradiation revealed that the onset of abrupt photo current occurs in less than 1 ms time scale. The GPPC in VO_2 device can contribute in realizing ultrafast optical remote control of advanced electronic devices i.e. optical memories, displays, and remote ultrafast switching devices.

1. Introduction

Persistent photoconductivity (PPC) is a phenomenon that refers to photo-induced conductivity that last for an extended time even after the photon source vanishes. PPC has been actively investigated in various materials, e.g. semiconductor heterostructures made of conducting GaAs on Cr-doped semi-insulating GaAs substrates, [1] AlGaAs/GaN, [2] Si nanomembranes, [3] metal oxides of WO_3 nanowire [4], $BaTiO_3/TiO_2$ heterostructures, [5] and even oxygen-deficient $YBa_2Cu_3O_{6+x}$ (YBCO) superconducting films. [6] While the origin of PPC in these materials comes from charge separation of photo-induced electrons and holes, the source of the charge separation seems to vary in each materials. In the case of semiconductors, the photo-induced carriers are separated due to potential barrier at the junction, the atomic scale of centers, or the surface. [1] In the case of oxides, the surface built-in potential contributes to the photo-generated electron–hole pairs that build potential barrier. [4] On the other hand, for the oxide superconductors, the charge separation occurs as photo-induced electrons from CuO_2 planes are trapped in the unoccupied p levels of O^- in CuO_x layers. [6]

Vanadium dioxide (VO_2), one of the well-known strongly correlated oxides exhibiting ultrafast massive insulator-to-metal transition (IMT) at near room temperature of 68 °C, has received much attention. [7] The full comprehension of IMT phenomena in VO_2 can provides the understanding of intricate physics of strongly correlated electron systems as well as the opportunities of diverse potential applications of VO_2 devices, such as ultrafast sensor, optical computing, and neuromorphic memories. [8–13] It is well known that the IMT of VO_2 can be induced by many different stimuli, e.g. temperature, voltage, light, and even strain. [14–17] While voltage-driven IMT in VO_2 device occurs from Joule heating that raises device temperature (T_D) to critical phase transition temperature (T_C), [18,19] a photo-induced IMT takes place due to photo-thermal heat. [20,21]

Especially, during the voltage-driven IMT, VO_2 exhibits hysteresis between two critical voltages $V_{IMT\uparrow}$ (critical voltage in increasing bias voltage) and $V_{MIT\downarrow}$ (critical voltage in decreasing bias voltage). When the bias voltage (V) is in the range of hysteresis loop $V_{MIT\downarrow} < V < V_{IMT\uparrow}$ (See Fig. S1 in Supplemental Information), a photo-irradiation can promote the photo-induced IMT on VO_2, i.e. the abrupt enhancement of photo-induced conductivity from the stable insulating low current state to metastable metallic high current state. In this case, a giant persistent photoconductivity (GPPC) can be realized [3–5] as the degree of PPC in VO_2 is quite large. Nevertheless, the occurrences of GPPC in VO_2 have hardly been investigated until now. Not to mention about in-

* Corresponding authors.
E-mail addresses: bsmun@gist.ac.kr (B.S. Mun), tesl@yonsei.ac.kr (H. Ju).

https://doi.org/10.1016/j.apmt.2020.100894

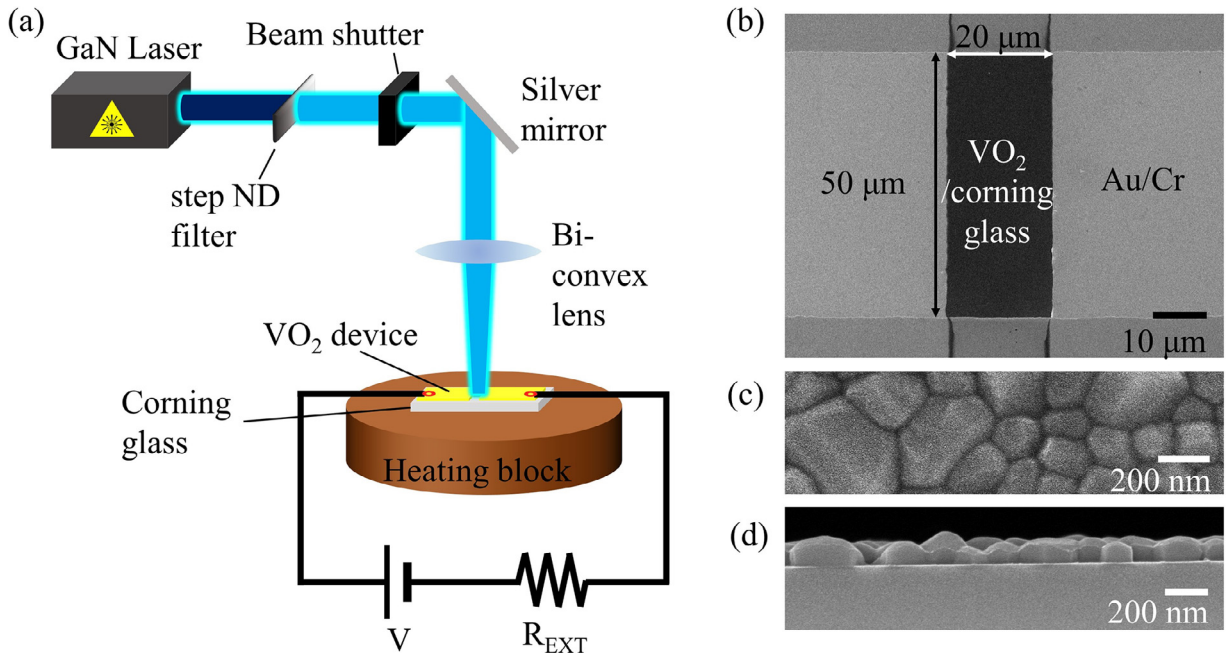

Fig. 1. (a) A schematic diagram of the experimental setup for the persistent photoconductivity measurements of the VO_2 devices with laser wavelength of 405 *nm* under varying photo irradiation time and laser intensities. (b) The scanning electron microscope (*SEM*) micrograph of a VO_2 device prepared on corning glass ($L = 20\ \mu$m, $W = 50\ \mu$m, thickness = 120 nm). (c) Top view SEM image of the VO_2/corning glass device. (d) Cross sectional SEM micrograph of the VO_2/corning glass device.

teresting transport properties at the viewpoint of the fundamental physics, the GPPC in VO_2 can promote numerous opportunities in technological applications of the VO_2 or related materials. Recently, a transient photoconductivity of VO_2 device and VO_2 internanowire junction are reported, in which the photocurrent exists temporary only when light is applied, and their high photo sensitivity for photo detection applications is noted. [22,23] It is also important to note that the GPPC in VO_2 comes from the laser induced phase transition of insulating state to metallic states. As mentioned previously, most of conventional GPPC materials comes from the photo-induced electrons and holes pairs that generates long-term charge separation inside of materials. [1–6]

In this letter, we report the GPPC of the two-terminal VO_2 device made of VO_2 film grown on corning glass substrate. Within the critical voltages of the voltage-current (V-I) hysteresis loop of the device, we showed that the GPPC of VO_2 device took place within as fast as ~ 1 ms upon a single pulse laser irradiation. The photo currents for VO_2 device were increased up to 1~5 mA and remained stable with only ~1% reduction over 24 h under the applied voltages of 7 V and 8 V. Optical microscope observation revealed that the GPPC in VO_2 was due to laser pulse induced IMT from stable low current state to metastable high current state. It was also discussed that the choice of low thermal conductivity substrate was of critical importance for the occurrence of GPPC.

2. Experimental details

The ~120 nm thick polycrystalline VO_2 films were deposited on corning glass (Eagle 2000) substrates by DC reactive magnetron sputtering system. The substrate temperature was maintained at 560 °C under mixed gas of argon 99% and oxygen 1% during deposition. A vanadium metal target was used and the films are cooled down in pure oxygen pressure of 50 mtorr after the deposition process. [24] The quality of VO_2 thin film was checked by X-ray diffraction and temperature dependent resistivity measurement, shown in Fig. S2 of Section 2 in Supplemental Information. The IMT temperature of VO_2, i.e. T_c was identified near ~67.8 °C. The VO_2 film devices made of VO_2 film on corning glass and Au(50 nm)/Cr(5 nm) contact electrodes were patterned by the standard photolithography and lift-off processes. The dimension of VO_2 device was 20 μm or 40 μm in length (L), the distance between the contact electrodes, at a fixed width (W) of 50 μm. The microstructure and morphology of VO_2 devices were characterized by scanning electron microscopy (SEM; JEOL-7610F-Plus). As shown in Fig. 1(a), during the PPC measurements, the VO_2 device was connected in series with an external resistor R_{EXT} (2 kΩ for $L = 20\ \mu$m device and 20 kΩ for $L = 40\ \mu$m device) to protect the VO_2 device and measuring instruments from the abrupt increase of photocurrent during IMT. A continuous 500 mW GaN laser diode with a wavelength of 405 nm was used. The laser power was controlled by a step neutral density (ND) filter and a laser pulse was made by opening and closing a laser beam shutter with opening time of ~800 μs (SH05, Thorlabs). [25] Laser intensity was checked with power meter (Nova II, Ophir Photonics). The laser was focused through a bi-convex lens and was applied vertically (except simultaneous long-term photo conductivity and optical microscopy measurements) onto the VO_2 film device via a silver mirror. With laser wavelength of 405 nm, the reflectivity (R_n) at normal incidence and absorption coefficient (α) of the VO_2 film were 0.2 and 1.2 $\times 10^5 cm^{-1}$, respectively. [26] Absorptance (A_n) at normal incidence was calculated from the equation $(1 - R_n)(1 - e^{-\alpha d})$, where d is the thickness (120 nm) of VO_2. [26] It was estimated that about 60% of the vertically irradiated laser beam on the VO_2 device was absorbed. On the other hand, during the simultaneous long-term photo conductivity and optical microscope image measurements, the single pulse laser irradiation was obliquely irradiated to VO_2 device at an angle of 60° from surface normal. Optical microscope with reflection mode was employed to monitor the metallic and insulating phases of VO_2 device before and after the single pulse laser irradiation. During V-I measurements under photo irradiation, the voltage was increased at a step of 0.01 V and the single pulse laser was irradiated at specific voltages for $V_{IMT\downarrow} < V < V_{IMT\uparrow}$. Voltage ramp rate during the V-I measurements was fixed to 0.03 V/s in which almost steady state is ensured within the film devices. Before the photo irradiation was made, the voltage ramping was stopped with 2 s of sta-

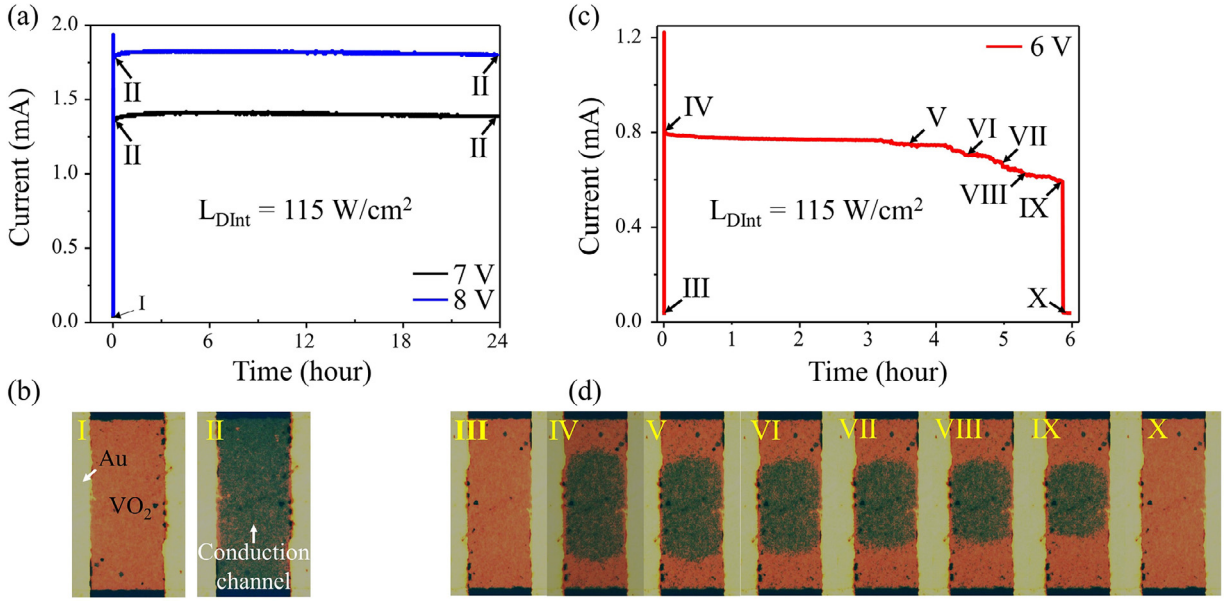

Fig. 2. Time dependence graphs of the persistent photo current (PPC) and optical microscope images of the VO_2/corning glass device as a function of time. The intensity of laser was set to L_{int} = 230 W/cm^2 and the ambient temperature was at 30 °C. A single pulse laser with its pulse width (L_{PW}) of 20 ms was irradiated while device of voltages (V) was set to 6 V, 7 V, and 8 V. The laser was obliquely irradiated at an angle of 60° from the surface normal of the VO_2/corning glass device. (a) The PPC curves at V = 7 V and 8 V. The photo current flowing in the VO_2 device remained almost constant at 1.3 mA at 7 V and 1.8 mA at 8 V. (b) The optical microscope images of the device at V = 7 V and 8 V. Upon the irradiation of single pulse laser, the color of optical images was changed from light-colored insulating phase (I) to dark-colored metallic state (II). The dark-colored metallic state (II) remained the same throughout the measurement. (c) The PPC at V = 6 V increased abruptly upon the laser irradiation, then started to decrease monotonically after ~3.5 h. After 5.8 h, the PPC dropped to the value of dark current. (d) The optical microscope images of the device at V = 6 V. The images showed decreasing channel width as photocurrents decreased in the order of III to IX. When the PPC drops to dark current value at X, the optical image returns to the original light-colored insulating state.

bilizing time. In the same manner, V-I measurements with photo-irradiation were repeated at different laser fluxes. The high-speed current (I)-time (t) measurements of VO_2 device with L = 20 μm were performed using a source meter (Keithley 2612A) with data collection rate up to 20,000 data per second.

3. Results and discussion

Shown in Fig. 1(a) is a schematic diagram of the experimental optical setup used in this study. The optical setup is consisted of a linearly polarized continuous 500 mW GaN laser diode, a step ND filter, an optical beam shutter, a silver mirror, and a bi-convex lens. The step ND filter is used to control laser intensity (L_{int}) from 140 W/cm^2 to 620 W/cm^2 at the VO_2 device position. Fig. 1(b) shows the SEM micrograph of VO_2/corning glass device with L = 20 μm and W = 50 μm, consisting of VO_2 film on corning glass substrate and Au/Cr electrodes. Fig. 1(c) shows the top view SEM image of the VO_2/corning glass film, which shows the film has grown into a densely packed granular structure with the average grain size of ~220 nm. Fig. 1(d) shows the cross-sectional SEM image of the VO_2 film /corning glass substrate, displaying the uniform thickness (~120 nm) of VO_2 with even interface with the corning glass substrate. It is also found that VO_2 grains are grown from the bottom to the surface without microstructure in column direction, which makes the average grain height and film thickness the same. The average lateral dimension of the grain, 220 nm, is almost twice the average grain height (or film thickness) of 120 nm.

To check out whether VO_2 can shows GPPC, the long-term photo conductivity and optical microscope measurements of the VO_2/corning glass device (W = 50 μm, L = 20 μm) were performed simultaneously at ambient temperature of 30 °C. A single pulse laser irradiation with pulse width (L_{PW}) of 20 ms was applied at the bias voltages of 6 V, 7 V, and 8 V. The laser with L_{int} = 230 W/cm^2 on the surface of the device was obliquely irradiated at an angle of 60° from the surface normal. In addition, to avoid any possible device deterioration during the extended measuring time under high voltage bias, experiments were performed with relatively low voltages of 6 V, 7 V, and 8 V.

Fig. 2(a) shows the time dependence of the photo-induced current (photo current) of the VO_2/corning glass device at the bias voltages of 7 V and 8 V. Indeed, GPPC in VO_2 was occurred abruptly with the single pulse laser. The magnitude of the photo current flowing in the VO_2 device remained fairly large, 1.3 mA at 7 V and 1.8 mA at 8 V, well above the base currents (0.05 mA-0.06 mA) before photo-irradiation. It is to note that the magnitude of the photo current can be increased further by reducing the magnitude of the external resistor R_{EXT}. When a single pulse laser was irradiated, the photo current was increased abruptly to more than one order of magnitude, followed by abrupt decrease of ~10% in magnitude. Then, the photo current decreased at a very slow rate, only 1.4% per day at 7 V and 1.1% per day at 8 V. Under the applied voltages of 7 V and 8 V, it was estimated that the high conductivity state could be persisted for several days, confirming that the photo current was highly stable at these applied voltages. When the applied voltage was sufficiently high (7 V, 8 V), the channel width was the same as the device width. But, when the applied voltage was low (6 V), the channel width became smaller than the device width, which was previously reported. [19] VO_2 undergoes transition from metal phase to insulating phase when the channel width is reached to the minimum width. In the case of a large initial channel width, e.g. high voltage bias case (7 V, 8 V), it takes a longer time to make the transition from metallic phase to insulating phase than that of a small initial channel width, e.g. low voltage bias case (6 V).

Since highly conductive metallic state is metastable, an equilibrium state, in which the metallic state remains stationary when the pulse is off, is believed to be nonexistent. That is, the photoinduced current eventually drops to the stable insulating value after suffi-

ciently long time. Nonetheless, at high applied voltages, the photoinduced current remains highly stable with extremely low decreasing rate. Also, we found that as the applied voltage increased, the slope of current reduction decreased. The possible origin is as follows: The super-cooled metallic grains, maintaining metallic phase even though temperature is lower than T_C, can transform to insulating grain. The phase transition probability from supercooled metallic grain to insulating grain drastically increases with the increasing $|T\text{-}T_C|$, where T is less than T_C. Since the device temperature increases when applied voltage increases, $|T\text{-}T_C|$ at large voltages is less than that at low voltages. [27] Therefore, the higher applied voltage induces higher device temperature, which then induce small rate of current reduction, as shown in Fig S6.

Next, Fig. 2(b) displays the optical microscope images of the VO_2/corning glass device ($W = 100\ \mu$m, $L = 20\ \mu$m) before and after laser pulse irradiation, which were simultaneously measured with Fig. 2(a), at the bias voltage of 7 V and 8 V. The color of the metallic phase VO_2 is darker than that of the insulating phase due to the difference of optical reflectivity. [14,28] Before the laser pulse irradiation, the microscope images at the bias voltage of 7 V and 8 V were the identical to the image I, displaying that the entire area of the device was the light-colored insulating phase. Then, after a single pulse laser irradiation, the entire area of the device turned into the dark-colored metallic phase, shown as image II. The change of surface color and abrupt current increase in VO_2 device indicated that the VO_2 film in the device experienced the IMT upon the laser irradiation, i.e. the IMT is the main cause of GPPC in the device.

To check out the correlation between photo conductivity in VO_2 caused by laser pulse and optical microscope images, the time dependence of the photo current of the VO_2/corning glass device at the slightly lower voltage, 6 V, was checked, shown in Fig. 2(c). Similar to the previous cases of the bias voltage of 7 V and 8 V, the photo current was increased abruptly with irradiation of a single pulse laser. However, the photocurrent started to decrease monotonically with irregular manner. At time of 5.8 hour, the current suddenly dropped to the dark current value (0.04 mA). Fig. 2(d) displays the optical microscope images of the VO_2/corning glass device ($W = 100\ \mu$m, $L = 20\ \mu$m) before and after laser pulse irradiation at the bias voltage of 6 V. Before the single pulse laser irradiation, the optical image at 6 V was the image III, thus the entire area of the device was insulating. After the single pulse laser irradiation, a dark colored metallic conduction channel with the channel width of 33 μm appeared suddenly between the two electrodes (optical image IV). Optical image IV showed the simultaneous presence of both insulating (light) and metallic (dark) phases. As time elapsed, optical microscopic images showed a decrease in channel width with decreasing photo currents. Then, the optical images changed to the order of V, VI, VII, VIII, and IX. When the channel width was reached to 23 μm (optical image IX), the conduction channel was suddenly collapsed and the photo current vanished. The optical image of position X, which was identical to the image III, showed that entire VO_2 was insulating. Thus, it is clear that the photo conductivity in VO_2 caused by laser pulse is directly related to the sudden appearance of the metallic phase, which can be present either in the entire area or partial area, depending on the applied voltage.

As the correlation between applied voltages and GPPC is shown to exist in the result of Fig. 2, it can be easily predicted that GPPC in VO_2 device is expected to occur only in the hysteresis region (Fig. S1). To check out the prediction, V-I measurements were performed first to find the hysteresis region of VO_2 device at given temperature and fixed laser flux. Once the hysteresis region of VO_2 is identified, multiple photo current states are generated afterward. First, Fig. 3(a) and (b) show the V-I measurements at 30 °C of the VO_2/corning glass devices with $L = 20\ \mu$m and $L = 40\ \mu$m at fixed $W = 50\ \mu$m. Again, while the VO_2 device with $L = 20\ \mu$m was connected to R_{EXT} of 2 kΩ, R_{EXT} of 20 kΩ was used for the VO_2 device of $L = 40\ \mu$m. This is due to smaller resistance of the VO_2 device of $L = 20\ \mu$m than that of the device of $L = 40\ \mu$m. The measurements were performed with the increasing and then decreasing bias voltage. For both devices, currents were increased continuously when the external voltage is applied from 0.0 V. The slope (dI/dV) was also increased with the increase of voltage. When the applied voltage on the VO_2/corning glass reached to $V_{IMT\uparrow}$ of 14.7 V (57.1 V) for the VO_2 devices with $L = 20\ \mu$m (40 μm), the currents suddenly jumped. When the bias voltage direction was reversed, the current in the device was decreased linearly until the voltage reaches the metal to insulator (MIT) voltage ($V_{IMT\downarrow}$) of 4.1 V (16.8 V) for the VO_2 device with $L = 20\ \mu$m (40 μm). Below the $V_{IMT\downarrow}$, current dropped rapidly and the VO_2 device became insulating state. Thus, the hysteresis regions of VO_2 device are identified, i.e. the region between $V_{IMT\downarrow}$ and $V_{IMT\uparrow}$. Next, GPPC experiments were conducted by applying single pulse laser to the VO_2 device between the lower and upper critical voltages.

Fig. 3(c) and (d) shows the V-I measurements of the VO_2/corning glass devices for $L = 20\ \mu$m and $L = 40\ \mu$m at fixed $W = 50\ \mu$m with single pulse laser irradiation at various voltages for $V_{IMT\downarrow} < V < V_{IMT\uparrow}$. During the V-I measurement, single pulse laser (L_{PW}=20 ms, $L_{int} = 140$ W/cm^2) was irradiated. In all cases, the GPPC is attained with a single pulse laser, within much shorter time than the laser pulse width of 20 ms. The magnitude of the photo-induced currents depended on the bias voltage: the higher the voltage, the greater the current. As predicted, GPPC started to show up inside the hysteresis region. It is interesting to note that GPPC tends to occur easily in VO_2 devices prepared on corning glass. Previously, GPPC was hardly reported in VO_2 devices prepared on Al_2O_3 substrate which is the most commonly used substrate for VO_2 film growth. The effect of substrates on the occurrence of GPPC needs further investigation in near future.

The giant persistent photoconductivity known so far is due to the photo-induced of electrons and holes. However, origin of GPPC found in VO_2 differ from that of GPPC in other materials. When the laser pulse is irradiated (Fig. 2(b)), the current is increased to 0.8 mA abruptly, and VO_2 becomes metallic. First, the carrier density of metallic state VO_2 is estimated at 0.8 mA. The mobility of VO_2 is reported as in the range 0.1 cm^2/Vsec - 1 cm^2/Vs with weak temperature dependence in the temperature range 20 °C and 100 °C, suggesting that the current increase predominantly due to the increase of carrier density. At IMT, the current is increasing by ~0.76 mA. If the mobility was assumed to be constant value of 1 cm^2/Vs in the temperature range 20 °C and 100 °C, the increased current density Δn is ~10^{20}/cm^3 from the relation $\Delta n = \frac{\Delta I}{Ae\mu E}$, where ΔI, e, μ, and E are the current increase, electron charge, the mobility of VO_2, and the electric field in VO_2, respectively. The calculated value matches well with reported value. [29] It is important to note that the magnitude of the estimated carrier density, i.e. the liberation of one electron per vanadium at the phase transition from insulating phase to metallic phase in VO_2, is much larger than the photoinduced carrier density of the GPPC materials. [30] Also, it is difficult to have the abrupt current density increase within 100μs, the time scale of via electron hole pair production with the single pulse of laser. Considering many of previous reports on PPC that based on photo-induced electrons and holes mechanism showed the continuous increase of the carrier density with the laser irradiation, the current density increase with a single pulse laser irradiation is not due to the electron hole pair generation.

To observe GPPC process of VO_2 device in details, e.g. the onset of GPPC, high-speed current (I)-time (t) measurements were performed. Fig. 4(a) show the high-speed I-t measurement results

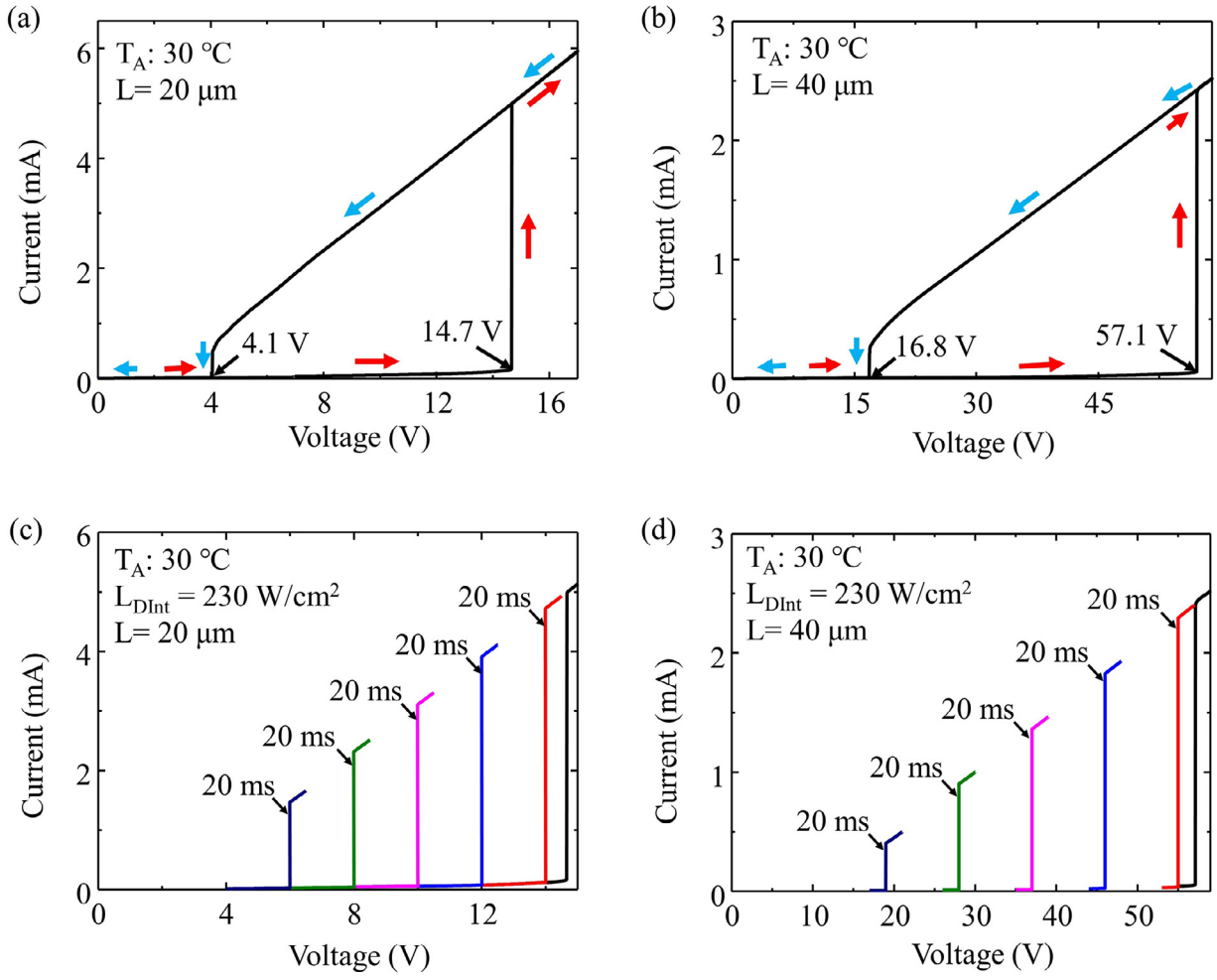

Fig. 3. (a, b) Voltage induced IMT measurements of the VO_2 / corning glass device with $L = 20\ \mu m$ and $40\ \mu m$ at fixed $W = 50\ \mu m$ without laser pulse irradiation. Red (Blue) arrow shows the increasing (decreasing) voltage scan direction. Insulator to metal transition (IMT), $V_{IMT\uparrow}$, occurred at 14.7 V in $L = 20\ \mu m$ (57.1 V in $L = 40\ \mu m$) and metal to insulator transition (MIT), $V_{IMT\downarrow}$, occurred at 4.1 V in $L = 20\ \mu m$ (16.8 V in $L = 40\ \mu m$). (c,d) The V-I measurements of the VO_2/corning glass devices for $L = 20\ \mu m$ and $L = 40\ \mu m$ at fixed $W = 50\ \mu m$ with single pulse laser irradiation at various voltages for $V_{IMT\downarrow} < V < V_{IMT\uparrow}$. During the V-I measurement, single pulse laser (L_{PW}=20 ms, L_{DInt} = 230 W/cm^2) was irradiated. The magnitude of the photo currents linearly increase with the value of the applied voltage.

for 20 μm long VO_2 film device at fixed bias voltage of 6 V with a single pulse laser at varying laser pulse intensity (L_{PW}=20 ms) from 140 W/cm^2 to 620 W/cm^2. With the single pulse laser irradiation, the photo current was increased from ~1.8 mA ~ 2.5 mA with the laser intensity from 140 W/cm^2 to 620 W/cm^2. The plot of photo current in Fig. 4(a) are divided into five regions. In region I, the current is constant as only the voltage is applied to the device without laser irradiation. In region II, the current started to increase with the laser pulse being applied. The IMT is not taking place in region II. The time, from the start of the current increase to the point where the device temperature reaches to T_c of VO_2 device, decreased from 1.2 ms to 0.6 ms as the laser intensity was increased from 140 W/cm^2 to 620 W/cm^2, shown in Fig. 4(b). The time, referred to as the incubation time (t_{inc}), has been also observed in voltage-induced IMT of epitaxial VO_2 devices and in threshold switching in VO_2. [31–33] The estimation process of t_{inc} is explained in Fig. S3(a, b) of Section 3 in Supplemental Information. In region III, the current rises rapidly due to the IMT and the current jump occurred in less than 100 μs. As the time taken for IMT (t_{IMT}) is related to the RC time of the device, RC time can be a critical component of t_{IMT} due to the internal bulk capacitance which can serve as a limitation to t_{IMT} due to charging/discharging effects. [34,35] In region IV, during the irradiation of the laser pulse, large photo currents with ripples were increasing over time. The ripple effect of the photo current is believed to be due to the voltage division between the resistor and the device. The device temperature is believed to increase in the region IV. In region V, as laser pulse was off, the photo current decreases throughout all four occasions. Fig. 4(c) show the high-speed I-t measurement results for 20 μm long VO_2 device at varying applied voltage at fixed laser intensity of 140 W/cm^2 (pulse width=20 ms). As the applied voltage is increasing, the current of VO_2 device is increasing linearly. The t_{inc} in Fig. 4(d) was decreased with the increasing the applied voltage from 1.2 ms at $V = 6$ V to 0.6 ms at 12 V. Also, the t_{IMT} was almost independent from the applied voltage and was about the similar value at all bias voltages, 100 μs.

In order to understand the origin of unique GPPC properties in VO_2 film device on corning substrate, important participating parameters are estimated, e.g. the temperature distribution over the device and substrate, steady state device temperature under the voltage bias, the incubation time, t_{inc}. First, the temperature distribution of the device and the substrate is estimated. When the laser is irradiated onto the VO_2 device during laser exposure time of sub ms to ~ ms, the heat from the surface is expected to be dissipated into the corning glass substrate up to tens of μm. Considering the thickness of the substrate (720 μm) is much thicker than that of VO_2 thin film (120 nm), we assume that one-dimensional approach

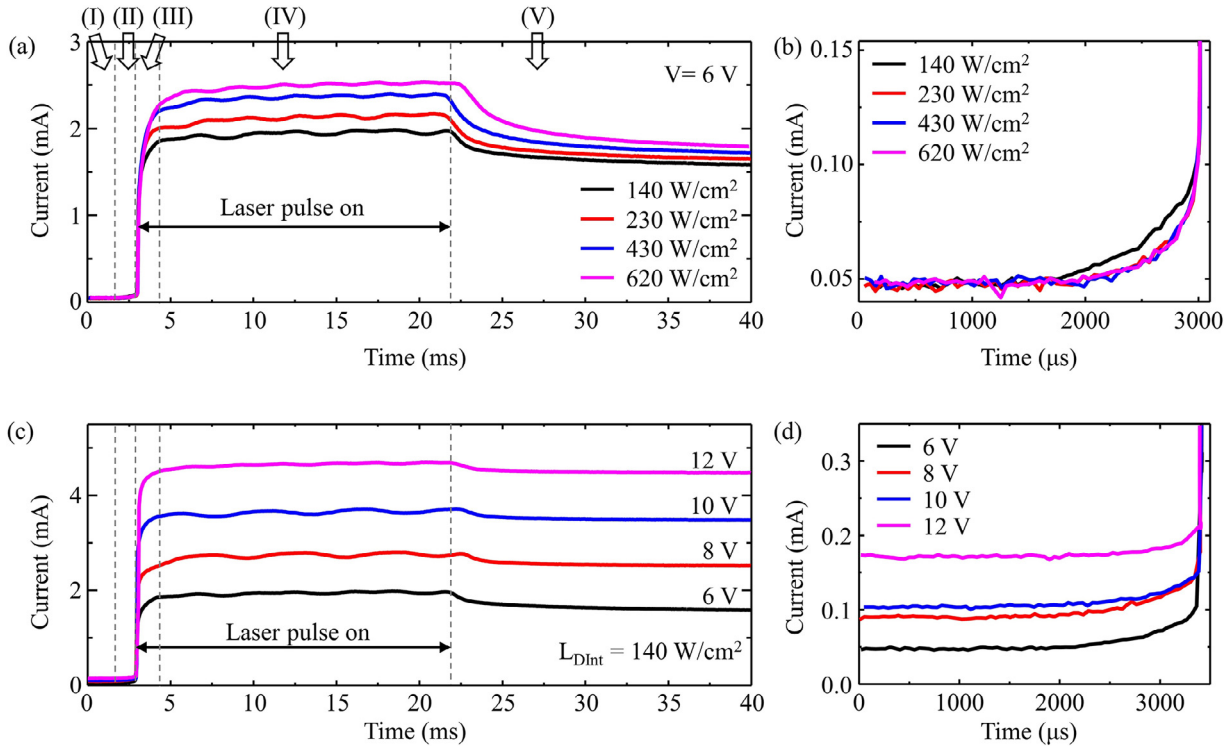

Fig. 4. (a) High speed current (I) - time (t) measurement for VO_2 device with $L = 20\ \mu m$ at fixed bias voltage of 6 V. The laser pulse width (L_{PW}) was 20 ms and the laser intensity (L_{PW}=20 was varied from 140 W/cm^2 to 620 W/cm^2. (b) Enlarged curve of the specified area in (a), just before abrupt current rise. (c) High speed current (I) - time (t) measurement for VO_2 device with $L = 20\ \mu m$ at varying voltages from 6 V to 12 V. The laser pulse width (L_{PW}) was 20 ms. The laser intensity was 140 W/cm^2. (d) Enlarged curve of the specified area in (c), just before abrupt current rise.

on the surface of a semi-infinite homogeneous solid medium is valid. (We will show later that our assumption on this point is valid.) It is also expected that the constant heat is generated at the surface and the heat conducts through the substrate. Then, the temperature distribution, i.e. temperature increment from steady state temperature, in the corning glass substrate can be given by, [36,37]

$$T(x,t) = \frac{I_0}{k_{corning}}\sqrt{\frac{\alpha_{corning}t}{\pi}}exp\left(-\frac{x^2}{4\alpha_{corning}t}\right) - \frac{I_0}{k_{corning}}\frac{x}{2}erfc\left(\frac{x}{2\sqrt{\alpha_{corning}t}}\right)$$

where I_0, $k_{corning}$, $\alpha_{corning}$, and x are a constant flux of energy, the thermal conductivity of corning glass, thermal diffusivity of corning glass, and the distance from interface between the VO_2 and substrate respectively. The $erfc$ is the complement error function. The temperature at $x = 0$ is given by $T(0,t) = \frac{I_0}{k}\sqrt{\frac{\alpha_{corning}t}{\pi}}$ and also $T(0,t)$ is approximately device temperature increment from steady state device temperature, shown in Fig. S4 of Section 4 in Supplemental Information. Then, the temperature in the corning glass can be written as;

$$T(x,t) = T(0,t)\left[exp\left(-\frac{x^2}{4\alpha_{corning}t}\right) - \sqrt{\pi}\frac{x}{2\sqrt{\alpha_{corning}t}}erfc\left(\frac{x}{2\sqrt{\alpha_{corning}t}}\right)\right]$$

Fig. 5(a) shows the $T(x,t)$ as a function of x which is the effective thermal diffusion length $\mu_{corning}$of corning glass $2(\alpha_{corning}t)^{1/2}$ [36], indicating that the temperature decreases to approximately 0.1 times from its surface value $T(0,t)$ at $x = \mu_{corning}$. Fig. 5(b) displays the time dependence of $\mu_{corning}$. When t is increasing from 1 μs and *1 ms*, $\mu_{corning}$ is increasing from 1.6 μm to 51 μm. That is, $\mu_{corning}$ at this time range is much larger than the film thickness (0.12 μm), which is supporting our assumption on one-dimensional approach on the surface of a semi-infinite homogeneous solid medium. Furthermore, since the substrate temperature was raised due to the conductive heat from the interface, the total heat energy transferred to the substrate can be obtained as follows,

$$\int_0^\infty c_{corning}\rho_{corning}AT(0,t)\left[exp\left(-\frac{x^2}{4\alpha_{corning}t}\right) - \sqrt{\pi}\frac{x}{2\sqrt{\alpha_{corning}t}}erfc\left(\frac{x}{2\sqrt{\alpha_{corning}t}}\right)\right]dx$$

After performing the integral, the above equation is equal to

$$\frac{c_{corning}\rho_{corning}AT(0,t)}{4}\sqrt{\pi}\mu_{corning}.$$

From this point of view, $T(0,t)$ becomes equal to $T_C - T_D$ in the relation of specific heat after the device temperature reaches T_C with the laser irradiation. (See Section 5 of Supplemental Information.) $T(0,t)$ is the temperature increment due to laser irradiation from steady state device temperature under bias voltage. This result will be used later for estimating incubation time, t_{inc}.

Next, we estimate the device temperature under bias voltage as IMT occurs in hysteresis regions. First, in the steady state, Joule heat IV_D in voltage biased VO_2 device without laser pulse irradiation is equal to thermally conductive heat loss $k_{eff}(T_D - T_A)$ through the substrate (neglecting other heat losses due to radiation and convection), where V_D (equal to $V - IR_{EXT}$), T_A, and k_{eff} are the voltage appeared on the VO_2 device, the ambient temperature

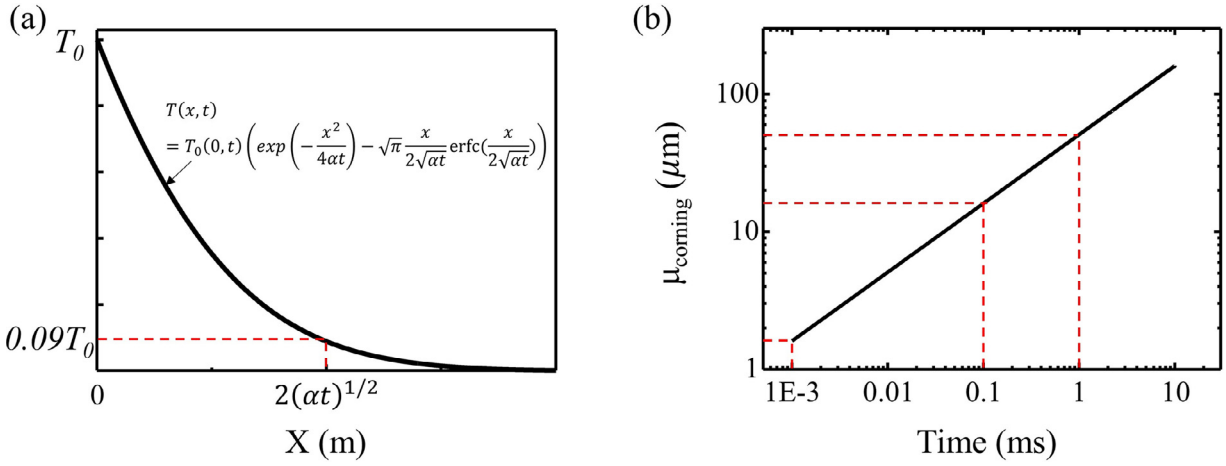

Fig. 5. (a) Transient temperature $T(x,t)$ in corning glass substrate as a function of the effective thermal diffusion length $\mu_{corning}$ of corning glass, defined as $2(\alpha_{corning}t)^{1/2}$. (b) The time dependence of the $\mu_{corning}$ in log scale.

Table 1
Calculated device temperature based on the photo thermalization model.

Voltage	6 V	8 V	10 V	12V
Device temperature	32.6 °C	34.9 °C	38.5 °C	44.1 °C

Table 2
Comparison between experimental and calculated incubation time as a function of laser intensity.

		140 W/cm^2	230 W/cm^2	430 W/cm^2	620 W/cm^2
Experiment	6	1.2 ms	0.6 ms	0.6 ms	0.6 ms
Calculation	V	2.4 ms	0.9 ms	0.3 ms	0.1 ms

Table 3
Comparison between experimental and calculated incubation time as a function of applied voltage.

		6 V	8 V	10 V	12 V
Experiment	140 W/cm^2	1.2 ms	0.8 ms	0.7 ms	0.6 ms
Calculation		2.4 ms	2.1 ms	1.7 ms	1.1 ms

and the effective thermal conductance, respectively. [19] Then, T_D is equal to $\frac{IV_D{}^2}{k_{eff}} + T_A$. The effective thermal conductance k_{eff} can be found when the device temperature is almost equal to T_C, just before IMT. Then, $k_{eff} = \frac{I_{DIMT-}V_{DIMT-}}{T_C - T_A}$, where I_{DIMT-} and $V_{DIMT-}$are the current flowing through the VO_2 device and the voltage appeared on the device immediately before IMT, respectively. We found the effective thermal conductance k_{eff} to be 6.6 $\times 10^{-5} W/^{\circ}C$ for the VO_2 device with $L = 20$ μm. Based on the calculated on effective thermal conductance k_{eff}, device temperature of the 20 μm long VO_2 device with applied voltages of 6 V, 8 V, 10 V, and 12 V were 32.6 °C, 34.9 °C, 38.5 °C, and 44.1 °C, respectively. (Table 1)

Finally, the incubation time is estimated. As previously discussed, the sum of two contributed heat energies can be written following. (See also Section 6 in Supplemental Information.)

$$\left[c_{VO2}\rho_{VO2}V_{VO2} + c_{corning}\rho_{corning}A\frac{\sqrt{\pi}}{4}\mu_{corning}\right](T_C - T_D).$$

As the volume contribution of the film is much smaller than the substrate, $V_{VO2} \ll A\mu_{corning}$, the equation becomes approximately to $c_{corning}\rho_{corning}A\frac{\sqrt{\pi}}{4}\mu_{corning}(T_C - T_D)$, which equals to $0.6L_{int}At_{inc}$. Then, the $\mu_{corning}$ can be described as $2(\alpha_{corning}t_{inc})^{1/2}$ and hence t_{inc}can be expressed as $t_{inc} = (\frac{c_{corning}\rho_{corning}(T_C - T_D)}{2 \times 0.6L_{int}})^2\pi\alpha_{corning}$. For the VO_2 device with $L = 20$ μm, the device volume, VO_2 density, specific heat capacity of VO_2 are 1.2 $\times 10^{-16} m^3$, 4.6 $\times 10^3 kg/m^3$, [38] and 6.6 $\times 10^2 J/kg^{\circ}C$, [39] respectively. Calculated t_{inc} is given in Table 2 and 3. The calculation values and experimental values are approximately within the same order. Overall, the calculated t_{inc}value varies large with the laser intensity, but less with applied voltage. The observation is believed due to that the assumption of one-dimensional heat flow is better applied with small t_{inc} than large t_{inc}. Recall that even when t_{inc} is 1 ms, $\mu_{corning}$ is *47* μm, comparable to the device dimension.

Considering the lower intensity at the initial opening time, the calculated t_{inc} can be adjusted in same order of magnitude with experiment. It is critical to note that the t_{inc} is proportional to thermal diffusivity, which is then proportional to thermal conductivity. The larger the thermal diffusivity becomes, the longer t_{inc} occurs. Thus, it reveals that GPPC can occur relatively easily for the substrate with a low thermal diffusivity (or low thermal conductivity). In fact, the switching time can be further reduced with the adjustment of laser intensity and RC time. First, to shorten the incubation time, the pulse laser with high intensity can be used. As the thermal diffusion length is shorter than the VO_2 thickness, most of the photo-thermal heat can be used to raise the VO_2 device temperature. Then, if the heat loss by the thermal conduction to the substrate is negligible, the incubation time can be obtained as follows.

$$(c_{VO2}\rho_{VO2}V_{VO2})(T_C - T_D) = 0.6L_{int}At_{inc}.$$

$$t_{inc} = \frac{(c_{VO2}\rho_{VO2}V_{VO2})(T_C - T_D)}{0.6L_{int}A}.$$

$V_{VO2} = At_{VO2}$, where t_{VO2} is the thickness of VO_2.

$$t_{inc} = \frac{(c_{VO2}\rho_{VO2}t_{VO2})(T_C - T_D)}{0.6L_{int}}.$$

The t_{inc} decreases as the L_{int} grows larger. When $L_{int}$is 2 $\times 10^6$ W/cm^2, t_{inc} is 1 ns. Secondly, as the time taken for IMT (t_{IMT}) is related to the RC time of the device, RC time can be a critical component of t_{IMT} due to the internal bulk capacitance which can serve as a limitation to t_{IMT} due to charging and discharging effects. Previously, it has been reported that RC time is proportional to L^2. [35] When the device length decreases to 1/300 times, the IMT time decreases to $1/(300)^2$ times. In the present device

IMT time is 100 μs. By reducing the device length 1/300 times from 20 μm to 67 nm, the IMT time is expected to be reduced down to ~1 ns. Thus, with further device optimization, the switching time, the sum of the IMT time and incubation time, can be as small as a few ns range.

The GPPC found in our VO_2 devices have three distinct differences from previous GPPC that occur in other materials or devices. First of all, the origin of GPPC is different from previously reported GPPC materials. i.e. the GPPC of VO_2 is due to IMT while the most of GPPC from other materials started out from electron-hole charge separation. Second, the GPPC of VO_2 occur rapidly with liberation of charges at IMT, yet the GPPC in other materials occurs relatively slow due the required sufficient time for photo generation of charges. Third, the GPPC of VO_2 is related to the metallic state, i.e. the magnitude of the current is larger than that of other materials. Until now, due to the limited magnitude of the photo current, GPPC phenomena have been mainly applied for simple light detection. However, in the case of VO_2, it becomes possible to operate various devices directly with the large current by the GPPC of VO_2. The photo current in VO_2 device can be increased up to tens of mA with the decreasing R_{EXT}. Furthermore, the device structure can be optimized so that the current passing through device becomes enlarged.

Lastly, the incubation time for reaching GPPC can be further controlled. With applying the laser pulse, the time needed for transition from insulator metal is the sum of incubation time and IMT time. While IMT time can be reduced by decreasing either R or C, e.g. IMT time can become as small as ns range, the incubation time can be reduced by increasing the laser intensity. In the case of ultrashort high intensity single pulse laser is applied to the device, most of the photo-thermal heat will be used to raise the device temperature as the thermal diffusion length within incubation time is very small. The higher the intensity of the laser, the shorter the incubation time. Consequently, the GPPC in VO_2 allows ultrafast remote optical control and manipulation of electric current and voltage, which can contribute in realizing the photo controlled electronic devices for optical memories and ultrafast remote switching devices.

Conclusions

We have investigated that GPPC of VO_2/corning glass device. A single pulse laser induced the GPPC of VO_2 device when the applied voltage was tuned between the two critical voltages in hysteresis region. The GPPC of VO_2 was monitored with the appearance of conduction channel on VO_2 devices during IMT. With the varying laser intensity or the applied voltage, the onset time for GPPC, i.e. incubation time, was varied. With one dimensional theoretical model, various thermal transport properties, i.e. the temperature distribution over the device, the incubation time, steady state device temperature under the voltage bias, were estimated. The GPPC in VO_2 can make a significant contribution to realization of optical control of electronic devices, e.g. optical memories, displays, and remote ultrafast switching devices.

Author statement

Gi Yong Lee: Conceptualization, Experiment, Formal analysis, Data Acquisition

Bongjin Simon Mun: Supervision, Writing-review & editing, Formal analysis

Honglyoul Ju: Methodology, Supervision, Writing-original draft, Funding, Project administration

Declaration of Competing Interest

The authors declare that they have no known competing financial interests or personal relationships that could have appeared to influence the work reported in this paper.

Acknowledgments

H. L. Ju and G. Y. Lee would like to thank the Basic Science Research Program for support through the National Research Foundation of Korea (NRF) funded by the Korean government (MOE) (NRF-2020R1F1A1061298, NRF-2018R1A6A3A01012528, NRF-2019R1I1A1A01041427). B. S. Mun would like to acknowledge the supports from the National Research Foundation of Korea (NRF-2015R1A5A1009962, NRF-2019R1A2C2008052) and the GIST Research Institute Grant funded by the Gwangju Institute of Science and Technology (GIST) 2020.

Supplementary materials

Supplementary material associated with this article can be found, in the online version, at doi:10.1016/j.apmt.2020.100894.

References

[1] H.J. Queisser, D.E. Theodorou, Hall-effect analysis of persistent photocurrents in n-GaAs layers, Phys. Rev. Lett. 43 (1979) 401–404 https://doi.org/10.1103/PhysRev Lett.43.401.
[2] J.Z. Li, J.Y. Lin, H.X. Jiang, M.A. Khan, Q. Chen, Persistent photoconductivity in a two-dimensional electron gas system formed by an AlGaN/GaN heterostructure, J. Appl. Phys. 82 (1998) 1227 https://doi.org/10.1063/1.365893.
[3] P. Feng, I. Mönch, S. Harazim, G. Huang, Y. Mei, O.G. Schmidt, Giant Persistent Photoconductivity in Rough Silicon Nanomembranes, Nano Lett. 9 (2009) 3453–3459 https://doi.org/10.1021/nl9016557.
[4] K. Huang, Q. Zhang, Giant persistent photoconductivity of the WO_3 nanowires in vacuum condition, Nanoscale Res. Lett. 6 (2010) 52 https://doi.org/10.1007/s11671-010-9800-1.
[5] M. Plodinec, A. Šantić, J. Zavašnik, M. Čeh, A. Gajović, Giant persistent photoconductivity in $BaTiO_3/TiO_2$ heterostructures, Appl. Phys. Lett. 105 (2014) 152101 https://doi.org/10.1063/1.4897999.
[6] V.I. Kudinov, I.L. Chaplygin, A.I. Kirilyuk, N.M. Kreines, R. Laiho, E. Lähderanta, C. Ayache, Persistent photoconductivity in $YBa_2Cu_3O_{6+x}$ films as a method of photodoping toward metallic and superconducting phases, Phys. Rev. B 47 (1993) 9017–9028 https://doi.org/10.1103/PhysRevB.47.9017.
[7] F.J. Morin, Oxides which show a metal-to-insulator transition at the neel temperature, Phys. Rev. Lett. 3 (1959) 34–36 https://doi.org/10.1103/PhysRevLett.3.34.
[8] E. Strelcov, Y. Lilach, A. Kolmakov, Gas sensor based on metal−insulator transition in VO $_2$ nanowire thermistor, Nano Lett. 9 (2009) 2322–2326 https://doi.org/10.1021/nl900676n.
[9] I. Olivares, L. Sánchez, J. Parra, R. Larrea, A. Griol, M. Menghini, P. Homm, L.-.W. Jang, B. van Bilzen, J.W. Seo, J.-.P. Locquet, P. Sanchis, Optical switching in hybrid VO_2/Si waveguides thermally triggered by lateral microheaters, Opt. Express 26 (2018) 12387 https://doi.org/10.1364/OE.26.012387.
[10] J.K. Clark, Y.-.L. Ho, H. Matsui, B. Vilquin, H. Tabata, J.-J. Delaunay, Photoinduced metal-like phase of VO_2 with Subns recovery, ACS Photon. (2020) acsphotonics.0c00280 https://doi.org/10.1021/acsphotonics.0c00280 .
[11] M. Rini, A. Cavalleri, R.W. Schoenlein, R. López, L.C. Feldman, R.F. Haglund, L.A. Boatner, T.E. Haynes, Photoinduced phase transition in VO_2 nanocrystals: ultrafast control of surface-plasmon resonance, Opt. Lett. 30 (2005) 558–560 https://doi.org/10.1 364/OL.30.000558.
[12] M. Liu, H.Y. Hwang, H. Tao, A.C. Strikwerda, K. Fan, G.R. Keiser, A.J. Sternbach, K.G. West, S. Kittiwatanakul, J. Lu, S.A. Wolf, F.G. Omenetto, X. Zhang, K.A. Nelson, R.D. Averitt, Terahertz-field-induced insulator-to-metal transition in vanadium dioxide metamaterial, Nature 487 (2012) 345–348 https://doi.org/10.1038/nature11231.
[13] H. Wang, X. Yi, Y. Li, Fabrication of VO_2 films with low transition temperature for optical switching applications, Opt. Commun. 256 (2005) 305–309 https://doi.org/10.1016/j.opt com.2005.07.005.
[14] B.S. Mun, K. Chen, J. Yoon, C. Dejoie, N. Tamura, M. Kunz, Z. Liu, M.E. Grass, S.-.K. Mo, C. Park, Y.Y. Lee, H. Ju, Nonpercolative metal-insulator transition in VO_2 single crystals, Phys. Rev. B. 84 (2011) 113109 https://doi.org/10.1103/PhysRevB.84.113109.
[15] Y. Zhou, X. Chen, C. Ko, Z. Yang, C. Mouli, S. Ramanathan, Voltage-triggered ultrafast phase transition in vanadium dioxide switches, IEEE Electron Device Lett. 34 (2013) 220–222 https://doi.org/10.1109/LED.2012.2229457.

[16] G. Seo, B.-J. Kim, Y. Wook Lee, H.-.T. Kim, Photo-assisted bistable switching using Mott transition in two-terminal VO_2 device, Appl. Phys. Lett. 100 (2012) 011908 https://doi.org/10.1063/1.3672812.
[17] J. Cao, Y. Gu, W. Fan, L.Q. Chen, D.F. Ogletree, K. Chen, N. Tamura, M. Kunz, C. Barrett, J. Seidel, J. Wu, Extended mapping and exploration of the vanadium dioxide stress-temperature phase diagram, Nano Lett. 10 (2010) 2667–2673 https://doi.org/10.1021/nl 101457k.
[18] B. Simon Mun, J. Yoon, S.-.K. Mo, K. Chen, N. Tamura, C. Dejoie, M. Kunz, Z. Liu, C. Park, K. Moon, H. Ju, Role of joule heating effect and bulk-surface phases in voltage-driven metal-insulator transition in VO_2 crystal, Appl. Phys. Lett. 103 (2013) 061902 https://doi.org/10.1063/1.4817727.
[19] J. Yoon, H. Kim, B.S. Mun, C. Park, H. Ju, Investigation on onset voltage and conduction channel temperature in voltage-induced metal-insulator transition of vanadium dioxide, J. Appl. Phys. 119 (2016) 124503 https://doi.org/10.1063/1.4944605.
[20] G.Y. Lee, B.S. Mun, H. Ju, Effect of photo-irradiation on metal insulator transition in vanadium dioxide, Appl. Phys. Lett. 113 (2018) 191902 https://doi.org/10.1063/1.5050880.
[21] J.M. Wu, L.B. Liou, Room temperature photo-induced phase transitions of VO_2 nanodevices, J. Mater. Chem. 21 (2011) 5499–5504 https://doi.org/10.1039/C0JM03203 D..
[22] B. Varghese, R. Tamang, E.S. Tok, S.G. Mhaisalkar, C.H. Sow, Photothermoelectric effects in localized photocurrent of individual VO_2 nanowires, J. Phys. Chem. C. 114 (2010) 15149–15156 https://doi.org/10.1021/jp1051936.
[23] B. Mukherjee, B. Varghese, M. Zheng, E.S. Tok, E. Simsek, C.H. Sow, Photoconductivity in VO_2-ZnO inter-nanowire junction and nanonetwork device, Nanosci. Nanotechnol. Lett. 8 (2016) 492–497 https://doi.org/10.1166/nnl.2016.2066.
[24] H. Kim, B.S. Mun, C. Park, H. Ju, Effect of over-oxidized surface layer on metal insulator transition characteristics of VO_2 films grown by thermal oxidation method, Curr. Appl. Phys. 17 (2017) 197–200 https://doi.org/10.1016/j.cap.2016.11.022.
[25] M. Vreugdenhil, D. Van Oosten, J. Hernandez-Rueda, Dynamics of femtosecond laser-induced shockwaves at a water/air interface using multiple excitation beams, Opt. Lett. 43 (2018) 4899–4902 https://doi.org/10.1364/OL.43.004899.
[26] T.V. Son, K. Zongo, C. Ba, G. Beydaghyan, A. Haché, Pure optical phase control with vanadium dioxide thin films, Opt. Commun. 320 (2014) 151–155 https://doi.org/10.1016/j.optcom.2014.01.037.
[27] R. Lopez, T.E. Haynes, L.A. Boatner, L.C. Feldman, R.F. Haglund, Size effects in the structural phase transition of VO_2 nanoparticles, Phys. Rev. B 65 (2002) 224113 https://doi.org/10.1103/PhysRevB.65.224113.
[28] J. Wei, Z. Wang, W. Chen, D.H. Cobden, New aspects of the metal–insulator transition in single-domain vanadium dioxide nanobeams, Nat. Nanotechnol. 4 (2009) 420–424 https://doi.org/10.1038/nnano.2009.141.
[29] D. Ruzmetov, D. Heiman, B.B. Claflin, V. Narayanamurti, S. Ramanathan, Hall carrier density and magnetoresistance measurements in thin-film vanadium dioxide across the metal-insulator transition, Phys. Rev. B 79 (2009) 153107 https://doi.org/10.1103/PhysRevB.79.153107.
[30] E. Arslan, S. Bütün, S.B. Lisesivdin, M. Kasap, S. Ozcelik, E. Ozbay, The persistent photoconductivity effect in AlGaN/GaN heterostructures grown on sapphire and SiC substrates, J. Appl. Phys. 103 (2008) 103701 https://doi.org/10.1063/1.2921832.
[31] D. Li, A.A. Sharma, D.K. Gala, N. Shukla, H. Paik, S. Datta, D.G. Schlom, J.A. Bain, M. Skowronski, Joule heating-induced metal-insulator transition in epitaxial VO_2/TiO_2 devices, ACS Appl. Mater. Interfaces. 8 (2016) 12908–12914 https://doi.org/10.1021/acsami.6b03501.
[32] G. Stefanovich, A. Pergament, D. Stefanovich, Electrical switching and Mott transition in VO_2, J. Phys. Condens. Matter. 12 (2000) 8837–8845 https://doi.org/10.1088/0953-8984/12/41/310.
[33] I.P. Radu, B. Govoreanu, S. Mertens, X. Shi, M. Cantoro, M. Schaekers, M. Jurczak, S. De Gendt, A. Stesmans, J.A. Kittl, M. Heyns, K. Martens, Switching mechanism in two-terminal vanadium dioxide devices, Nanotechnology 26 (2015) 165202 https://doi.org/1 0.1088</number> /0957-4484/26/16/165202.
[34] G.Y. Lee, H. Kim, B.S. Mun, C. Park, H. Ju, Investigation on I-V characteristics of current induced metal insulator transition in VO_2 device, Curr. Appl. Phys. 17 (2017) 1444–1449 https://doi.org/10.1016/j.cap.2017.08.006.
[35] A. Kar, N. Shukla, E. Freeman, H. Paik, H. Liu, R. Engel-Herbert, S.S.N. Bhardwaja, D.G. Schlom, S. Datta, Intrinsic electronic switching time in ultrathin epitaxial vanadium dioxide thin film, Appl. Phys. Lett. 102 (2013) 072106 https://doi.org/10.1063/1.4793537.
[36] Carslaw and Jaeger, Conduction of heat in solids (1959) (ISBN 0198533683).
[37] S.K. Lau, P. Almond, P.M. Patel, Transient thermal wave techniques for the evaluation of surface coatings, 24 (1991) 428–436. https://doi.org/10.1088/0022-3727/24/3/029.
[38] H. Wen, L. Guo, E. Barnes, J.H. Lee, D.A. Walko, R.D. Schaller, J.A. Moyer, R. Misra, Y. Li, E.M. Dufresne, D.G. Schlom, V. Gopalan, J.W. Freeland, Structural and electronic recovery pathways of a photoexcited ultrathin VO_2 film, Phys. Rev. B 88 (2013) 165424 https://doi.org/10.1103/PhysRevB.88.165424.
[39] C.N. Berglund, H.J. Guggenheim, Electronic properties of VO_2 near the semiconductor-metal transition, Phys. Rev. 185 (1969) 1022–1033 https://doi.org/10.1103/PhysRev.185.1022.